Vacancy-solute interactions during ageing of a cold worked Mg-RE alloy

Fabio Moia, Rafael Ferragut, Alberto Calloni, Alfredo Dupasquier, Carlos Eugenio Macchi, Alberto Somoza, Jian-Feng Nie

Vacancy-solute interactions during ageing of a cold worked Mg-RE alloy

Journal:	*Philosophical Magazine & Philosophical Magazine Letters*
Manuscript ID:	TPHM-09-Oct-0443.R1
Journal Selection:	Philosophical Magazine
Date Submitted by the Author:	15-Dec-2009
Complete List of Authors:	Moia, Fabio; Politecnico di Milano, Dipartimento di Fisica Ferragut, Rafael; Politecnico di Milano, Dipartimento di Fisica e Centro L-NESS Calloni, Alberto; Politecnico di Milano, Dipartimento di Fisica Dupasquier, Alfredo; Politecnico di Milano, Dipartimento di Fisica Macchi, Carlos; Universidad Nacional del Centro de la Provincia de Buenos Aires, Departamento de Física Somoza, Alberto; Universidad Nacional del Centro de la Provincia de Buenos Aires, Departamento de Física Nie, Jian-Feng; Monash University, Department of Materials Engineering
Keywords:	magnesium alloys, positron annihilation, precipitation
Keywords (user supplied):	

Vacancy-solute interactions during ageing of a cold worked Mg-RE based alloy

F. Moia[a], R. Ferragut[a§], A. Calloni[a], A. Dupasquier[a], C.E. Macchi[b], A.Somoza[c] and J. F. Nie[d]

[a] *Dipartimento di Fisica, LNESS and CNISM, Politecnico di Milano, Via Anzani 42, I-22100 Como, Italy;* [b] *IFIMAT, UNCentro and CICPBA, Pinto 399, B7000GHG Tandil, Argentina;* [c] *IFIMAT, UNCentro and CONICET, Pinto 399, B7000GHG Tandil, Argentina;* [d] *Department of Materials Engineering, Monash University, Victoria 3800, Australia.*

[§] Corresponding author. E-mail: rafael.ferragut@polimi.it

(Received 23 October 2009; final version received 15 December 2009)

The vacancy–solute interactions during artificial ageing at 250°C of cold worked samples of a commercial magnesium alloy WE54 (Mg-RE based) were studied by coincidence Doppler broadening of positron annihilation radiation and positron annihilation lifetime spectroscopy. The results show that in the as-cold-worked state the vacancies are associated with dislocations that are generated by the cold work, and that after artificial ageing at 250°C the vacancies are associated with solute elements and help the formation of precipitate precursors. This mechanism accelerates the formation of hardening precipitates without any apparent changes in the precipitation sequence and in the products of the decomposition of the supersaturated solid solution. The present study demonstrates that the stronger hardening response achieved in the cold worked samples originates from the presence of a higher concentration of vacancies that is introduced by the cold work and is retained in the first few minutes of ageing.

Keywords: Magnesium alloys; Positron annihilation; Precipitation.

1. Introduction

Precipitation hardening is known to occur in magnesium alloys containing rare-earth elements during artificial ageing of these alloys at elevated temperatures [1]. This phenomenon effectively contributes to the improvement of mechanical properties of this class of magnesium alloys [2,3]. The precipitation sequence and the morphology of the hardening precipitate phases are relatively well established for commercial alloys that are based on the Mg-Y-RE (rare-earth) system, e.g. WE43 and WE54

alloys [4-9]. An important microstructural factor influencing the nucleation and growth of the strengthening precipitate phases in these age-hardenable alloys is the nature of lattice defects. In the specific case of WE54, which is the alloy selected for study in the present work, it has been reported that cold work after solution treatment and water quench and before artificial ageing at 200°C and at 250°C, can accelerate and enhance the age hardening response [10,11]. This effect is clearly shown by the hardening curves reported in Ref. [11] that are reported in Figure 1 in the present paper for the convenience of readers. The beneficial effect of cold work on age hardening enhancement is also well known for aluminum based alloys (e.g., [12,13]).

Figure 1 about here

In order to gain deeper understanding of the interplay between solute atoms and open volume defects (vacancies and vacancy-like defects that are located in disordered regions and at interfaces) in the WE54 alloy, positron annihilation lifetime spectroscopy has been used by Macchi *et al.* [11]. The propensity of the positrons to be trapped by open volumes inside solids makes positron annihilation lifetime spectroscopy the most sensitive technique for observing vacancy-like defects and the evolution of their density during structural transformation of alloys (for further information on positron annihilation lifetime spectroscopy studies of metallic alloys, see Ref. [14]). Coincidence Doppler broadening (CDB) of the positron annihilation radiation is another positron-based technique which can sensitively detect the identity of open volume defects and it is specially suited for identifying the nature of vacancy-solute aggregates. The CDB technique is based on the measurement of the shape of the positron annihilation line at 511 keV with a very high signal/noise ratio ($\approx 10^5$), which leads to the determination of the momentum distribution of the electrons taking part in the positron annihilation. The shape of the electronic momentum contains

specific signatures of the chemical species probed by the positrons at the annihilation site [15]. This technique is now widely used for an approximated chemical analysis of vacancy-solute aggregates in light alloys (an example with full details on the methodology is given in Ref. [16]).

The CDB measurements of artificially aged, undeformed samples of the same alloy have been reported in Ref. [17]. These measurements reveal the almost total absence of frozen-in vacancies in the as-quenched condition and suggest that only thermal equilibrium vacancies contribute to solute transport. In the present work, the positron annihilation study is extended to deformed (cold worked) specimens. These additional data and their comparison with the results reported in Refs. [11,17] give us the opportunity to shed light on the mechanism in which deformation-induced defects influence precipitation.

2. Experimental procedures

2.1 Sample preparation

The samples were taken from a cast plate of WE54 (Magnesium Elektron Company, England), with a nominal composition of Mg - 5.1Y- 3.3RE - 0.4Zr (wt.%), where RE stands for a mixture of Nd and heavy rare-earth elements, with Nd as the main component. The samples were solution treated for 8 hours at 525°C, quenched in water at room temperature and immediately cold rolled to a thickness reduction of 6% and 12%. After a dwell time of a few days at room temperature (this alloy is not prone to natural ageing at room temperature), the samples were artificially aged at 250°C for up to 4 hours. The ageing treatment was temporarily interrupted during positron annihilation measurements. The interruption entailed water quenching followed by a short exposure at room temperature before 24 hours dwelling at liquid nitrogen

temperature. In the text below, the effect of artificial ageing interruption is neglected and the accumulated dwell time at 250°C is taken as the effective ageing time.

2.2 Positron annihilation lifetime spectroscopy

Positron annihilation lifetime measurements published in Ref. [11] were performed at room temperature. Since the positron trapping rate in the diffusion-controlled regime – see below – depends on the temperature, room temperature lifetime data cannot be directly correlated with momentum spectra taken at the liquid nitrogen temperature. New lifetime spectra have thus been collected simultaneously with momentum spectra by using a plastic (Pilot U, start) and a BaF_2 (stop) scintillator aligned at 90° from the axis of the Ge detectors, with the sample mounted on the cold finger of a cryostat at the centre of the cross. The resolution of the lifetime spectrometer was 257 ps, and the count rate in this case was 5 s^{-1}. The number of counts was 4×10^5 per spectrum. All spectra were analysed using the POSITRONFIT program [18] in one component after source subtraction. Since the spectra are expected to contain two or more unresolved components, the result of one-component fits must be intended as an effective average lifetime.

2.3 Coincidence Doppler broadening (CDB) of the annihilation radiation

All measurements were taken at the liquid nitrogen temperature simultaneously with lifetime spectra, as explained above, by means of two hyperpure Ge gamma detectors coupled to a multiparametric pulse analyser. Background rejection was achieved by requiring time coincidence within a window of 300 ns and fulfilment of the energy conservation condition $|E_1 + E_2 - 2m_0c^2| < 2.1$ keV, where E_1 and E_2 are the energies

measured by the two detectors respectively. The component along the axis joining the two detectors of the momentum of the annihilating pairs is given by $p_L = \frac{E_1 - E_2}{c}$

The momentum resolution was 3.7×10^{-3} m_0c. Twenty millions counts were collected in each spectrum. The analysis of the momentum spectra $\rho(p_L)$ was carried out, as explained in Refs. [16, 17], by fitting a linear combination of momentum spectra measured in the same experimental condition for pure elements, as given by the following function:

$$\rho = (1-\mathrm{F})\,\rho_{Mg}^{bulk} + \mathrm{F}\left(\mathrm{C}_{Mg}\rho_{Mg}^{V} + \mathrm{C}_{Y}\rho_{Y}^{V} + \mathrm{C}_{Nd}\rho_{Nd}^{V} + \mathrm{C}_{Zr}\rho_{Zr}^{V}\right), \quad (1)$$

where the fitting parameters are the trapping fraction F (relative number of positrons that are trapped and annihilated in open volume defects) and the fractional concentrations C_{Mg}, C_Y, C_{Nd}, and C_{Zr}. Here it should be noted that the above fractional concentrations are to be interpreted as representing (with a possible distortion, due to the different positron affinity for the different elements [19] and to the lattice relaxation) the atomic composition in regions that are in immediate contact with the vacancy where the positron is trapped. It must be emphasised that the local composition in contact with a defect can differ from the average composition of the vacancy–solute aggregates. In Eq. 1, ρ_{Mg}^{bulk} is the experimental momentum distribution for bulk Mg measured from an annealed Mg with 99.9 % purity; ρ_{Mg}^{V}, ρ_{Y}^{V}, ρ_{Nd}^{V}, ρ_{Zr}^{V} are the momentum distributions expected for annihilation in vacancies in pure elements, as obtained from measurements on cold worked samples after subtracting the contribution of annihilations from free positrons [16]. In our approximated analysis the contribution of rare-earths mixed to Nd is assumed to be included in the Nd term. The shape of the Mg bulk spectrum ρ_{Mg}^{bulk} is shown in Figure 2. The

momentum distributions ρ_X^V for saturated positron trapping at vacancies (X = Mg, Y, Zr, and Nd) are reported in Figure 3 as relative differences $\frac{\rho_X^V - \rho_{Mg}^{bulk}}{\rho_{Mg}^{bulk}}$ to the spectrum of Figure 2. Note that the vertical scale of the upper frame in Figure 3 is amplified by an order of magnitude for helping the visibility of the small signal given by trapping at vacancies in Mg. In order to eliminate uncertainties in the analysis of CDB spectra, a two-step fitting procedure was used. In the first step, free fits were used to determine the value of the trapping fraction F and its error as an average over a series of different fits giving approximately the same χ^2. In the second step, the F value was kept as a constraint.

Figures 2 and 3 about here

3. Experimental results and discussion

3.1 Positron annihilation lifetime results

The evolution of the positron lifetime during ageing is shown in Figure 4 for the cold worked samples. For the purpose of comparison, results obtained from undeformed samples are also included in this figure. The horizontal axis of Figure 4 represents the ageing time normalised at the peak hardness ageing time (see arrows in Figure 1) which is equal to 22 h and 42 min, 5 h and 37 min and 3 h and 20 min respectively for the 0%, 6% and 12% deformations). The scaling of the time axis of Figure 4 corroborates that the deformation treatment affects the kinetics of the decomposition process without noticeable changes in the sequence of different stages of the precipitation process. Full symbols represent lifetime data taken at the liquid nitrogen temperature simultaneously with the CDB measurements. Open symbols are the lifetime data taken at room temperature for the same samples used by Macchi *et al.*

[11]. The two sets of data are almost coinciding in the as-quenched condition and at the beginning of the heat treatment, but at later ageing stages the low temperature data are systematically above the room temperature data. This difference is consistent with positron trapping in a coarse distribution of extended defects like incoherent precipitates, which usually have open spaces at their interfaces with the magnesium matrix. In these conditions, referenced in the positron annihilation literature as diffusion-limited regime, the increase in the positron diffusion constant occurring at low temperature [20] enables a larger fraction of positrons to reach the traps. The lowering of the positron lifetime at long ageing times, which is more evident at room temperature than at the liquid nitrogen temperature, certifies that the average distance between positron trapping sites is of the order of the positron diffusion length, i.e. typically 100 nm at room temperature, and tends to increase with ageing time.

Figure 4 about here

3.2 Coincidence Doppler Broadening results

The momentum spectra $\rho(p_L)$ of the annihilation radiation are shown in Figure 5 in terms of the ratio-difference function

$$\Delta = \frac{\rho - \rho_{Mg}^{bulk}}{\rho_{Mg}^{bulk}}, \qquad (2)$$

where ρ_{Mg}^{bulk} is the CDB spectrum measured for bulk Mg shown in Figure 2. This representation is used to enhance the details of the spectra in the high-momentum region, which is most important for the identification of the chemical species in contact with vacancy-like defects. Note that, for a fixed chemical composition of the environment of the positron traps, the curves scale vertically in proportion to the trapping fraction *F*. The symmetrical experimental curves have been folded around

p_L= 0. The statistical noise has been reduced by averaging groups of three subsequent points from 1 to 2.6 atomic momentum units and of six points above 2.6 atomic units. The solid lines through the experimental data are the best-fit curves obtained in accordance with the procedure described in Sec. 2.3.

Figure 5 about here

The parameter of the fit that gives direct information on the density of open volume defects is the trapping fraction *F*. Figures 6a, 6b and 6c show that *F* is strongly correlated with the lifetime measured at the same temperature. The consistency of *F* data obtained from the CDB measurements with independent positron lifetime results is a good test for the reliability of the linear model adopted for the CDB analysis. Most importantly, the lifetime changes are essentially determined by concomitant changes of the trapping fraction, with minor or no influence by the local chemistry at the annihilation site.

Figure 6 about here

In the undeformed samples, the positron trapping is very weak (3%) after quenching and remains so even after 15 min at 250°C. On the contrary, the cold work increases the initial fraction of trapped positron by about 60% in the less deformed (6%) samples and near 70% in the more severely deformed (12%) samples. However, a very short heating leads to a sharp drop of the positron trapping. For example, for the 12% deformed samples the trapping fraction falls to about 15% after only 90 s at 250°C. After this initial decrease in positron trapping, further evolution of precipitation towards peak ageing entails an apparent increase in *F* by about 90%, which is then followed by a slight decrease in the case of the cold worked samples. As discussed above for the lifetimes, the decrease in positron trapping at long ageing time is due to coarsening of the precipitate distribution. As this effect is not seen in the

undeformed sample, one can conclude that in this case, where the evolution is slower than that in the case of cold work, the precipitates are still dense at the scale of the positron diffusion length after 4 days at 250°C. However, this indication is not consistent with the lifetime data; thus the small rise of F at long ageing time might come from an imperfect fitting.

Additional information on the positron traps is given by the chemical composition of their environment. Figure 7 shows the total solute concentration probed by the trapped positrons, as given by the sum of the fitting parameters $C_{sol} = C_Y + C_{Nd} + C_{Zr}$, as a function of the ageing time scaled in proportion to the hardness peak time. This figure demonstrates that the intense trapping observed at the beginning of the ageing treatment is dominantly due to vacancy-like defects embedded in the Mg-rich matrix, without relevant decoration by solute ($C_{sol} \approx 0$); this is opposite to the case of undeformed samples, where trapping is very weak and is due to vacancies deeply embedded in solute (C_{sol} near to 100%).

Figure 7 about here

Heating for 15 min does not substantially change both the local solute concentration and the trapping fraction in the undeformed sample. On the contrary, in the 12% deformed sample a short ageing of 90 s at 250°C rises the local solute concentration up to above 50%, in concomitance with a drop in the trapping fraction at its minimum of 15%. A jump is observed also for the less deformed (6%) sample after 15 min ageing (this sample was not tested at 90 s). It may be argued that the heating leads to rapid migration and loss of a large fraction of the vacancies that are introduced by the cold work. There is, however, a non-negligible fraction that survives and appears to be bound to solute clusters in an environment that is even richer in solute than expected for the stoichiometric compositions of the β', β_1 and β

phases. It may be concluded that only the vacancies that are not stabilised by clustering with solute atoms are rapidly removed by heating.

Continuing the heat treatment makes the solute fraction gradually converge in all cases to an asymptote just below 20%. The asymptote is reached more or less in coincidence with peak hardening, when β', β_1 and β precipitates are densely distributed in the material as shown in the TEM images displayed in Figure 8.

Figure 8 about here

The information regarding the concentration of each solute species at the annihilation site is the following. Zr is positively identified only in the undeformed sample after quenching or after short ageing (15 min), when trapping is very small (F= 3%). In accordance with the interpretation given in Ref. [17], this result indicates that, in the absence of competition by other traps, a small fraction of positrons can reach and become trapped in sparse Zr dispersoids. The interesting information that can be drawn from this finding is that, in the undeformed material, after quenching and some dwelling time at room temperature, there are almost no free vacancies or vacancy-solute clusters containing Y and Nd, which in the model adopted in the present analysis, represents approximately all rare earths. On the contrary, these elements become well recognisable when the intensification of trapping indicates the beginning of precipitation. Figure 9 depicts the Y fraction $C_Y / C_Y + C_{Nd} + C_{Zr}$. These data indicate that, excluding the pre-ageing conditions, the relative proportions of Y and Nd stay approximately constant in a ratio between 1:1 and 3:2 during the entire development of the ageing process (the horizontal line in Figure 9 is drawn at 58% that is the average value of the Y fraction for all samples, excluding the initial points).

Figure 9 about here

4. Conclusions

For cold worked samples of magnesium alloy WE54, the combined evidence of positron lifetime and CDB measurements makes it possible to distinguish a succession of three stages of the precipitation process during ageing at 250°C**:**

a) *dissolution of free vacancies and formation of precipitate precursors*: the majority of vacancies associated with the dislocations introduced by cold work are removed after a few minutes at 250°C (only 90 s for 12% deformation, see the drop in the positron lifetime and in the trapping fraction documented in Figures 4 and 6); the residual vacancies give rise to the formation of vacancy-solute aggregates where the environment of the vacancies is richer in solute than expected for the β', β_1 and β precipitate phases (see the sudden initial jump in the solute fraction displayed in Figure 7);

b) *precipitation*: the formation of precipitate phases β', β_1 and β is accompanied by an increase in the density of vacancy-like positron traps (see in Figures 4 and 6 the increase of the positron lifetime and of the trapping fraction that takes place after the initial drop and is extended up to about the hardness peak time); the progressive transformation of solute-rich clusters in more stable phases occurs at about 20% of the peak hardness time, as shown by the change of the local chemistry near to the positron traps documented in Figure 7.

c) *coarsening*: continuing the heat treatment beyond peak hardening leads to an increase in the average distance between open volume defects, which is sensed by positrons as a reduction in the lifetime measured at room temperature and,

less evidently, by the lifetime and CDB parameters measured at the liquid nitrogen temperature (Figures 4 and 6).

In conclusion, the present study demonstrates that the stronger hardening response that is achieved by applying cold work prior to artificial ageing comes from a residual population of vacancies that is produced by the cold work and not annealed in the first minutes of ageing. These vacancies are stabilised by association with solute atoms and help the formation of precipitates precursors. This action accelerates the formation of hardening precipitates without evident changes in the precipitation sequence and in the products of the decomposition of the initial supersaturated solid solution.

References

[1] L.L. Rokhlin, *Magnesium Alloys Containing Rare Earth Metals: Structure and Properties*. Taylor & Francis, London, 2003.

[2] I.J. Polmear, Mater. Sci. Technol. 10 (1994) p. 1.

[3] I.J. Polmear, *Light Alloys: From Traditional Alloys to Nanocrystals*. 4th Ed, Butterworth-Heinemann, Oxford, 2006.

[4] J.F. Nie and B.C. Muddle, Scripta mater. 40 (1999) p. 1089.

[5] J.F. Nie and B.C. Muddle, Acta mater. 40 (2000) p. 1691.

[6] C. Antion, P. Donnadieu, F. Perrard, A. Deschamps, C. Tassin and A. Pisch, Acta mater. 51 (2003) p. 5335.

[7] C. Antion, P. Donnadieu, C. Tassin and A. Pisch, Phil. Mag. 86 (2006) p. 2797.

[8] P. Mengucci , G. Barucca , G. Riontino , D. Lussana ,M. Massazza, R. Ferragut and E. Hassan Aly, Mater. Sci. Eng. A 479 (2008) p. 37.

[9] G. Riontino, M. Massazza, D. Lussana, P. Mengucci, G. Barucca and R. Ferragut, Mater. Sci. Eng. A 494 (2008) p. 445.

[10] T. Hilditch, J.F. Nie and B.C. Muddle, *Magnesium Alloys and their Applications*, B.L. Mordike and K.U. Kainer, eds., Wolfsburg, Germany, 1998, p. 339.

[11] C. E. Macchi, A. Somoza and J. F. Nie phys. stat. sol. (c) 4 (2007) p. 3538.

[12] R. Ferragut and A. Somoza, phys. stat. sol. (a) 175 (1999) p. R1.

[13] A. Tolley, R. Ferragut and A. Somoza, Phil. Mag. 89 (2009) p. 1095.

[14] A. Dupasquier, G. Kögel and A. Somoza, Acta Mater. 52 (2004) p. 4707.

[15] P. Asoka-Kumar, M. Alatalo, V. J. Gosh, A. C. Kruseman, B. Nielsen and K.G. Lynn, Phys. Rev. Lett. 77 (1996) p. 2097.

[16] A. Dupasquier, R. Ferragut, M.M. Iglesias, M. Massazza, G. Riontino, P. Mengucci, G. Barucca, C.E. Macchi and A. Somoza, Phil. Mag. 87 (2007) p. 3297.

[17] F. Moia, A. Calloni, R. Ferragut, A. Dupasquier, C.E. Macchi, A. Somoza and J.F. Nie, Z. Metallkd. 100 (2009) p. 378.

[18] P. Kirkegaard, N.J. Pedersen and M. Eldrup: PATFIT-88, M-2740, Risø National Laboratory, Risø, 1989.

[19] A. Calloni, A. Dupasquier, R. Ferragut, P. Folegati, M.M. Iglesias, I. Makkonen and M. Puska, Phys. Rev. B 72 (2005) 054112.

[20] B. Bergersen, E. Pajanne, P. Kubica, M.J. Stott and C.H. Hodges, Solid State Commun. 15 (1974) p. 1377.

Figure captions

Figure 1: Vickers hardness as a function of the ageing time at 250°C (after Ref. [11]).

Figure 2. Momentum distribution spectrum for annealed Mg.

Figure 3. Momentum distribution spectra for pure Mg, Y, Nd, Zr in conditions of high positron trapping at vacancies (relative difference to the spectrum of Figure **2** corresponding to annealed Mg).

Figure 4. Mean positron lifetime as a function of the normalised ageing time (i.e., scaled in proportion to the hardness peak time) in cold worked and undeformed samples. Full symbols: room temperature (RT) measurements (after Ref. [11]). Open symbols: liquid nitrogen temperature (LNT) measurements (this work). The solid lines are for visual guide.

Figure 5. Annihilation radiation spectra (relative difference to bulk Mg) in cold worked and undeformed samples at various ageing times. Solid lines: linear combination model.

Figure 6. Comparison between the average positron lifetime (full symbols) and the trapping fraction *F* (open symbols) deduced from CDB data obtained from cold worked and undeformed samples vs. the ageing time. All measurements were performed at liquid nitrogen temperature.

Figure 7. Solute fraction probed by the trapped positrons at the annihilation site in deformed and cold worked samples vs. the normalised ageing time. The solid lines are for visual guide.

Figure 8. Transmission electron micrographs showing microstructuress typical of (a) 6% deformed samples aged for 8 hours at 250°C and (b) 12% deformed samples aged at 250°C for 4 hours.

Figure 9. Ratio between Y and total solute atomic concentrations probed by the trapped positrons in cold worked and undeformed samples vs. the normalised ageing time.

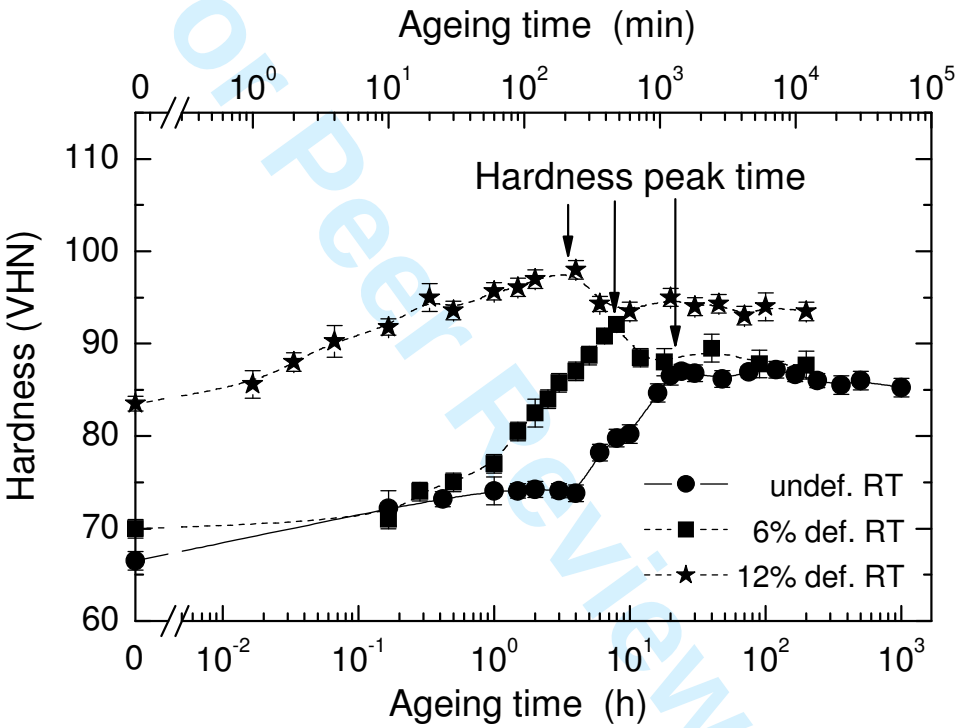

Figure 1

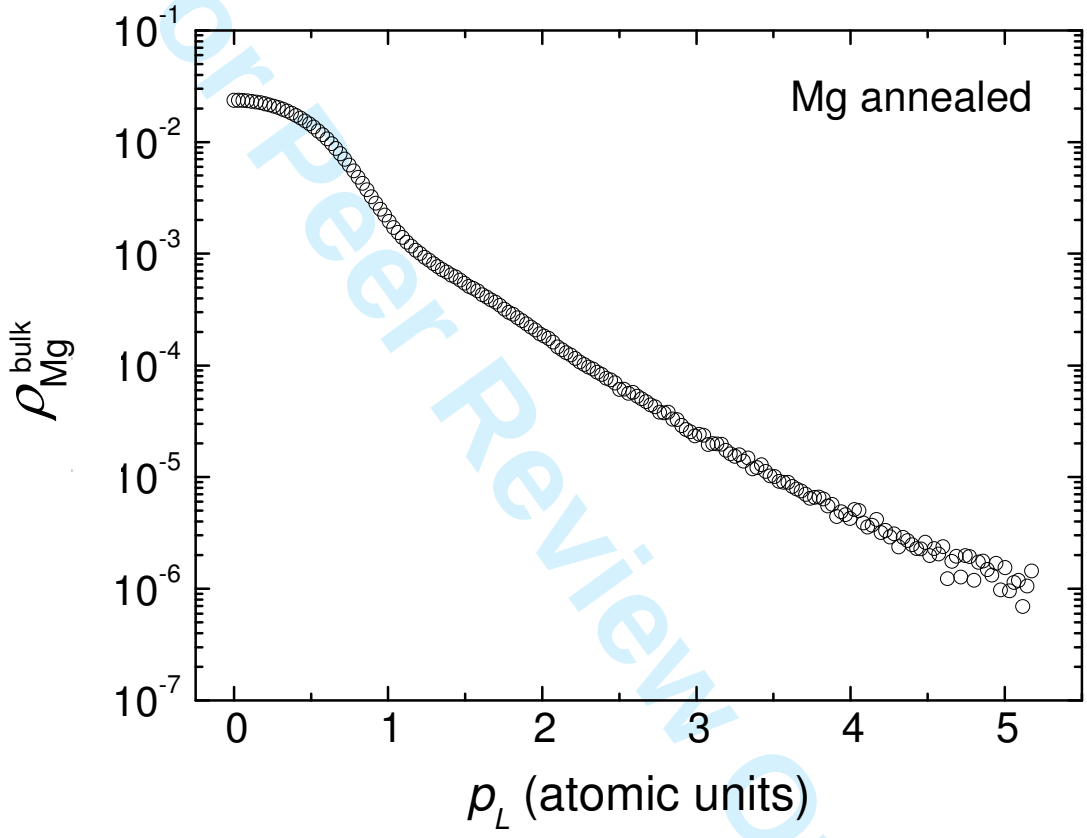

Figure 2

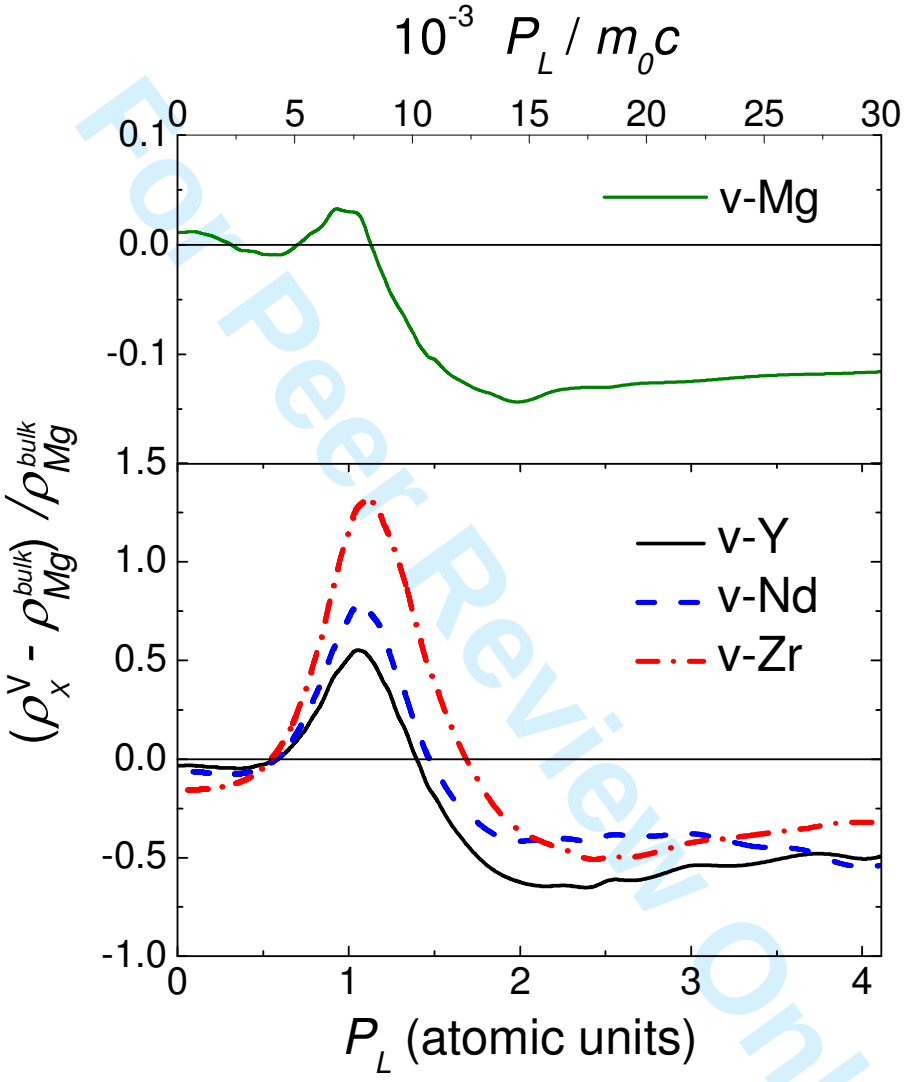

Figure 3

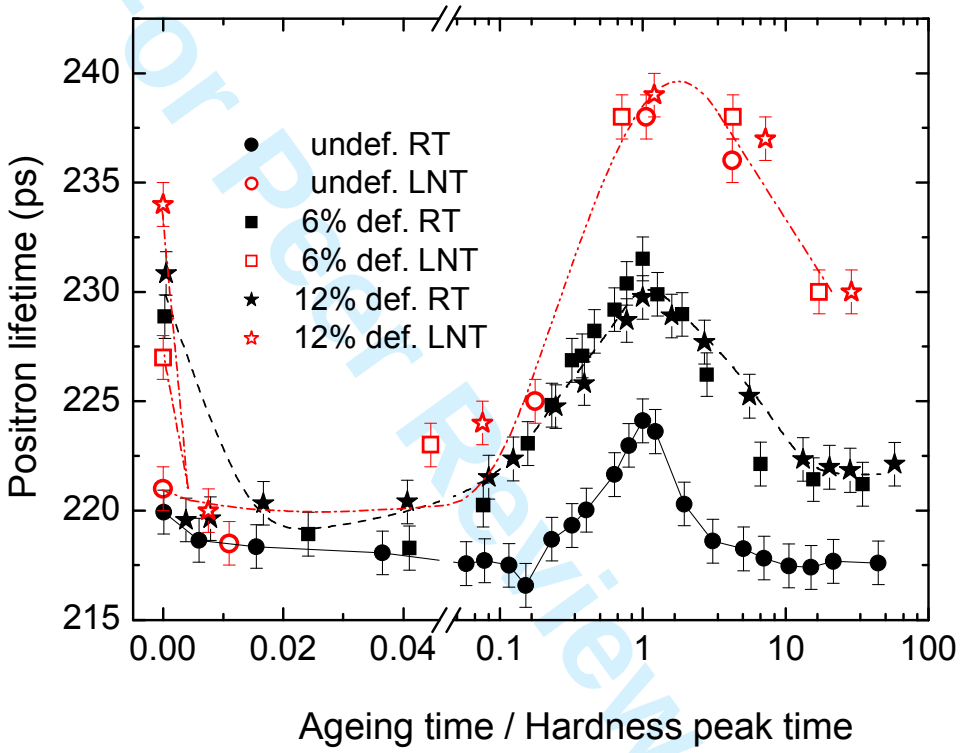

Figure 4

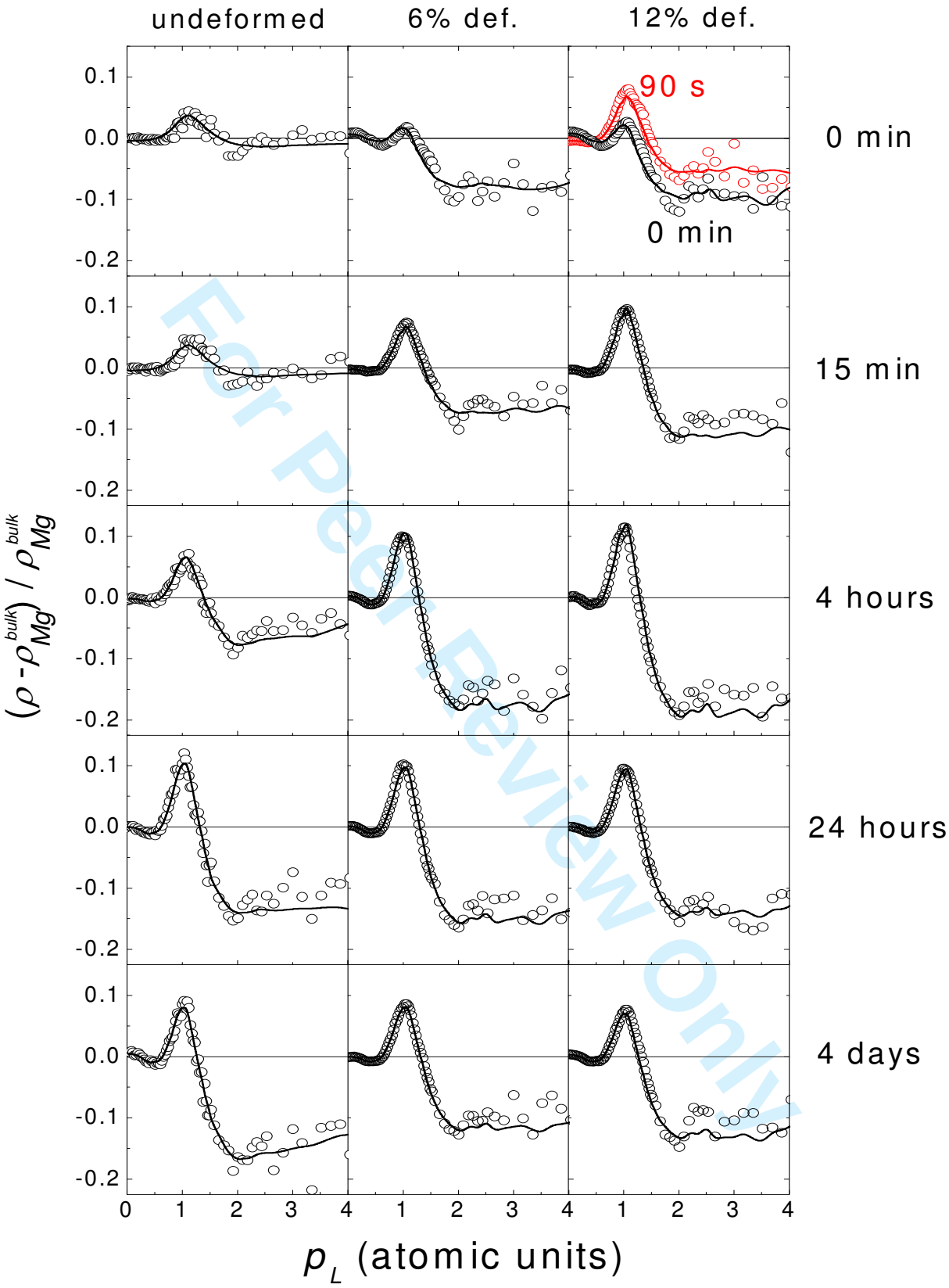

Figure 5

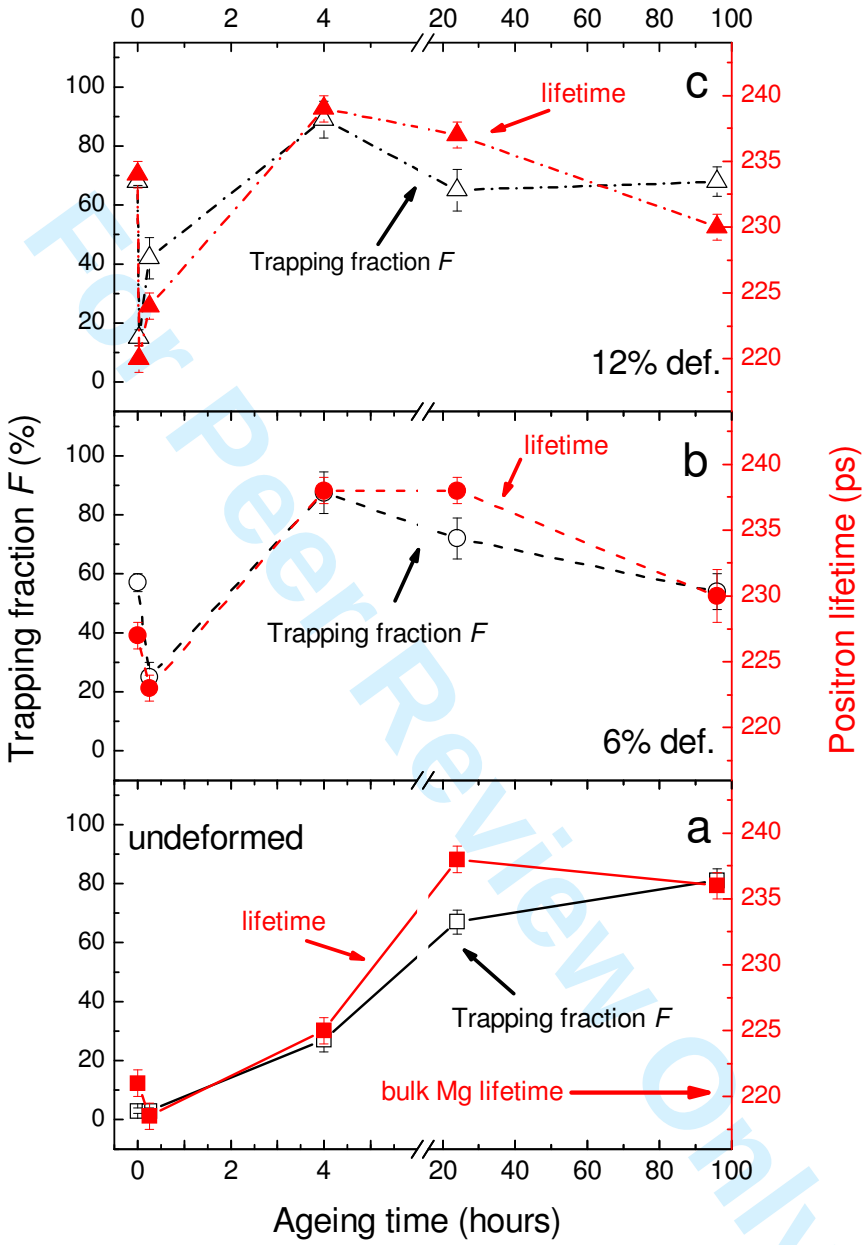

Figure 6

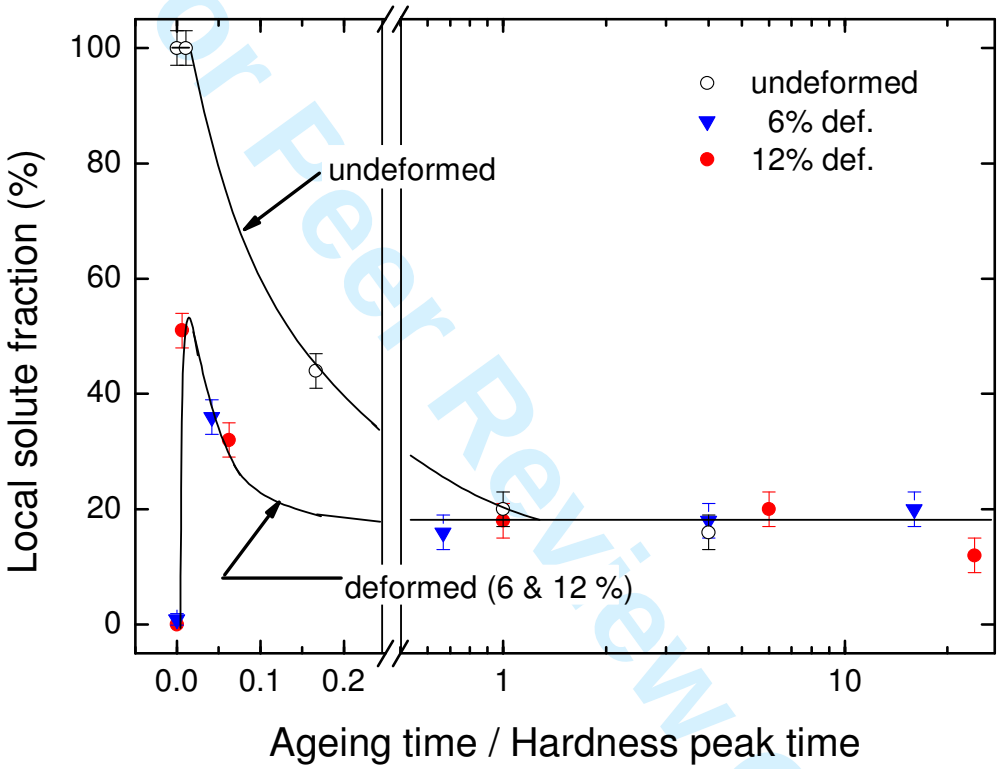

Figure 7

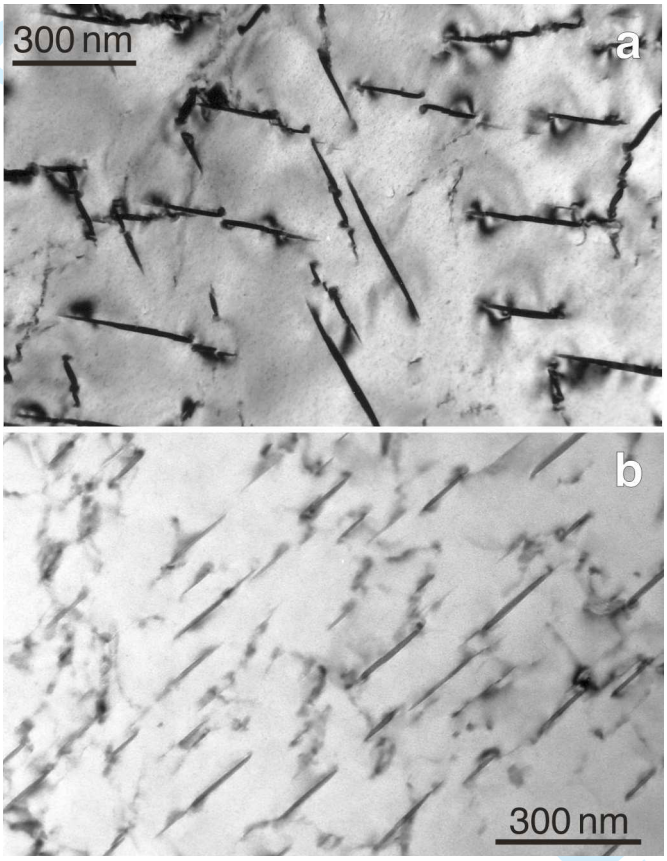

Figure 8

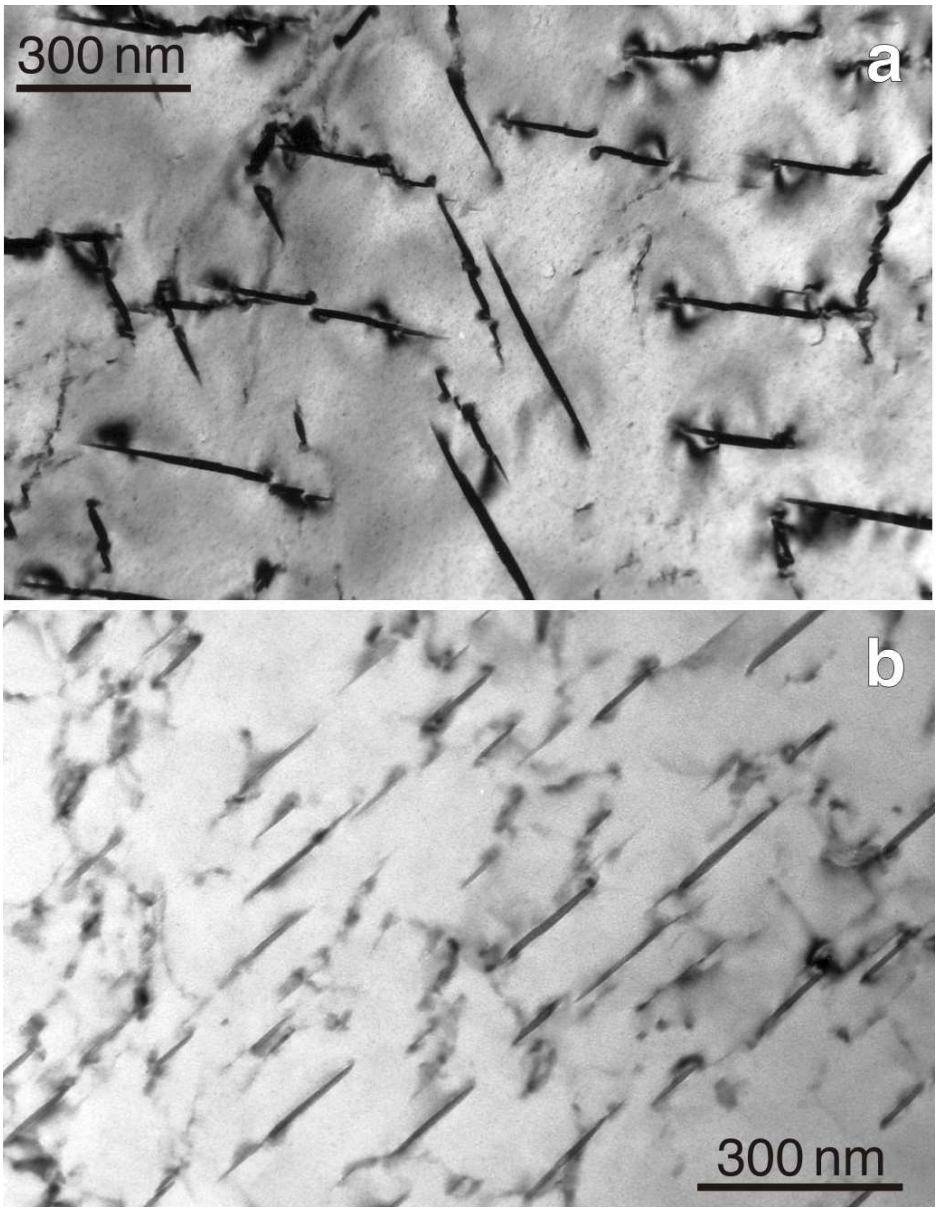

Transmission electron micrographs showing microstructuress typical of (a) 6% deformed samples aged for 8 hours at 250°C and (b) 12% deformed samples aged at 250°C for 4 hours.

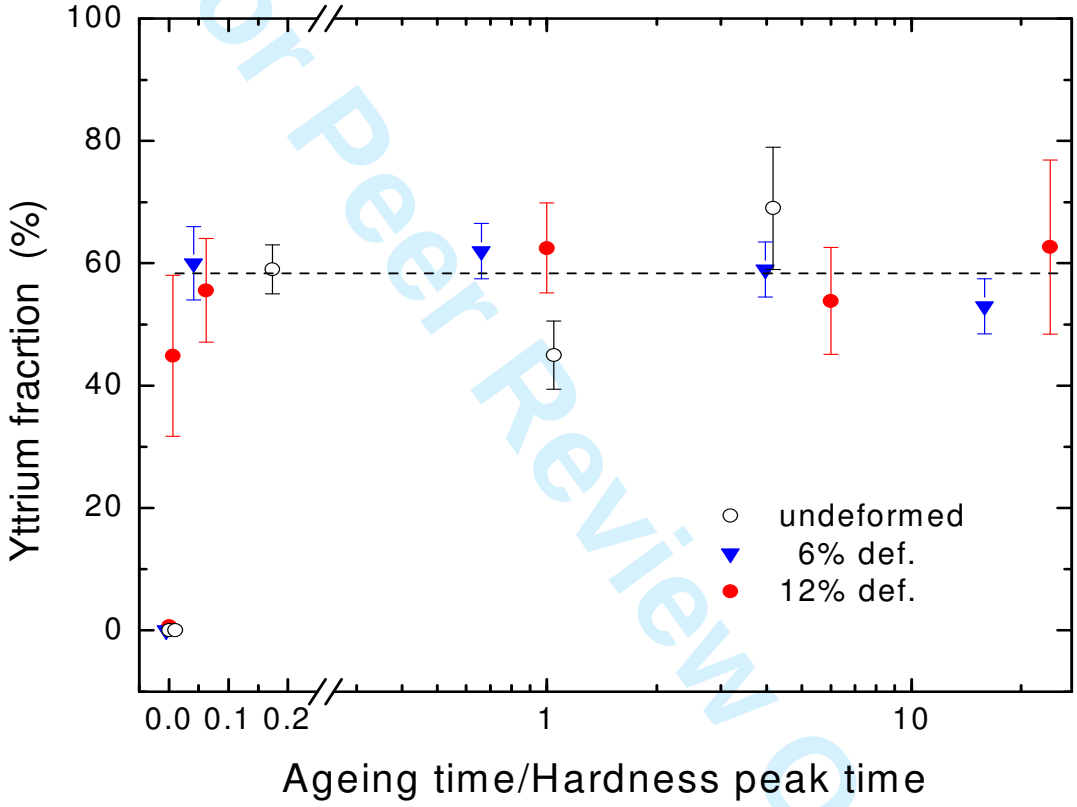

Figure 9